Improving the strength and surface properties of TNTZ alloy through a combination of high-pressure torsion and laser surface treatment

Hsuan-Kai Lin[1*], Tsai-Hsuan Hsieh[1], Yi-Hong Cheng[1], Piotr Bazarnik[2], Chuan Ting Wang[3], Yi Huang[4,5*], Jing Ye[4], Amor Abdelkader[4], Terence G. Langdon[5]

[1]Department of Materials Engineering, National Pingtung University of Science and Technology, Pingtung 912, Taiwan
[2]Warsaw University of Technology, Faculty of Materials Science and Engineering, Woloska 141, 02-507, Poland
[3]School of Mechanical Engineering, Nanjing University of Science and Technology, Nanjing 210094, Jiangsu, PR China
[4]Department of Design and Engineering, Faculty of Science and Technology, Bournemouth University, Poole, Dorset BH12 5BB, UK
[5]Materials Research Group, Department of Mechanical Engineering, University of Southampton, Southampton SO17 1BJ, UK
* Correspondent author: Hsuan-Kai Lin (HKLin@mail.npust.edu.tw)
Yi Huang (yhuang2@bournemouth.ac.uk)

Abstract

The Ti–29Nb–13Ta–4.6Zr alloy (TNTZ) is a β-Ti alloy that has a potential for use in biomedical applications as an alternative to the less-compatible Ti64 alloys. Enhancing the strength and the surface finish of TNTZ is essential for biomedical applications. In this research, a combination of high-pressure torsion (HPT) and laser treatment was used to improve the TNTZ properties. The HPT-treated samples showed significantly enhanced mechanical properties when compared with the traditional solution-treated TNTZ. A laser surface treatment immediately forms a hydrophilic surface that transforms into a steady hydrophobic state after 14 days in air and the surface roughness increases with an increase in laser power and a slower scanning rate. The corrosion resistance of TNTZ improves significantly after laser treatment, with the corrosion current dropping from 1×10^{-8} A to 1.2×10^{-9} A and the corrosion potential peak shifting to a more positive value from -0.349 V to -0.158 V. The friction coefficient after laser treatment decreased from 0.134 to 0.093 and then further reduced to 0.082 after 14 days in air thereby suggesting an enhancement in the tribological properties. Overall, the results show that HPT processing combined with a post-HPT laser treatment is beneficial for enhancing the mechanical properties and the corrosion and wear performance of the TNTZ alloy.

Keywords: electrochemistry; high-pressure torsion; hydrophobicity; laser surface modification; TNTZ alloy.

1. Introduction

Commercial titanium alloys have high mechanical strength, good biocompatibility and excellent corrosion resistance. As a result, they are widely used in biomedical applications such as in orthopedics and stomatology. However, in the Ti64 alloy, which is one of the most extensively used titanium alloys, the Al and V elements are cytotoxic and can lead to problems such as Alzheimer's disease and nervous system disorders [1, 2]. Consequently, β-Ti alloys, which consist mainly of Ta and Nb, have attracted much attention in recent years due to their superior biocompatibility and their overall safety in the human body [3]. In addition, the elements Ta and Nb in β-Ti alloys can form stable Ta_2O_5 and Nb_2O_5 films at the surface that effectively prevent electron exchange and therefore produce excellent corrosion resistance [4-6]. Some β-Ti alloys, such as Ti-Nb-Ta-Zr (TNTZ) alloys, exhibit a low Young's modulus and hence they are exceptionally suitable for use as implant materials [7-10]. However, the tensile strength of β-Ti alloys is much lower by comparison to the commonly used T64 alloy. Therefore, it is important to improve the strength of β-Ti alloys while maintaining the favorable low value of Young's modulus.

The mechanical performance of biomedical materials can be improved by thermomechanical processing and microstructure control to achieve a refined grain size [11]. For Ti alloys, the most effective processing method for grain refinement is high-pressure torsion (HPT) which can produce an ultra-fine grain structure and improve the mechanical strength [12, 13]. Notably, there are reports that grain refinement can also improve the corrosion resistance [14]. Many studies have shown that hydrophobic surfaces have favorable self-cleaning and corrosion-resistance properties [15]. Surface modification technologies such as laser ablation and electrodeposition that produce high-energy metal oxides prompt a gradual change in the surface properties from hydrophilic to superhydrophobic over time [15, 16]. Moreover, such technologies can also improve the biological activity of the surface by inducing favorable cell arrangements or directional growth [17, 18]. The TNTZ alloy is particularly suited to biomedical applications due to its superior corrosion resistance and biocompatibility compared to other Ti alloys [19-22]. Thus, HPT processing and laser treatment are expected to further

enhance the strength and improve the resistance to corrosion and wear of the TNTZ alloy. Therefore, the present study was conducted to investigate the synergistic effects of high-pressure torsion and laser surface modification on strength, surface characteristics, corrosion performance and wear performance. The effectiveness of the proposed approach is demonstrated using solution-treated samples for comparison purposes.

2. Experimental material and procedures

The TNTZ alloy used in this research was a Ti–29Nb–13Ta–4.6Zr ingot produced by melting the pure elements together in the correct proportions under a purified Ar atmosphere. The ingots were solution treated at 800°C for 2 hr in a protected gas Ar atmosphere in order to remove casting defects such as component segregations. Disk samples with a diameter of 10 mm and thickness of 1.0 mm were wire-cut from the solution-treated ingots and these disks were ground on both faces using abrasive papers to remove the surface layers affected by the wire-cutting process. The final thickness of the ground disk samples was around 0.8 mm. The disks were individually processed by HPT for 1, 5 and 20 turns, respectively, at 25°C with an applied pressure of 6.0 GPa and a rotational speed of 1 rpm. The HPT process was conducted under a quasi-constrained configuration to prevent excessive material flow from around the periphery of the disk in the gap between the upper and lower anvils [23]. For consistency, the samples that were solution treated but without HPT processing were designated as N0 samples whereas those solution treated and further processed by HPT with 1, 5 and 20 turns were denoted as N1, N5 and N20, respectively.

The microstructures of samples in the solution treated and HPT-processed conditions were examined with an Olympus BX51 optical microscope (OM) after grinding, polishing and etching with etchant (16 ml HF+64 ml HNO_3+800 ml H_2O). The microstructure of the N20 sample was further characterized using a JEOL1200 transmission electron microscope (TEM) operating under an accelerating voltage of 120 kV. All TEM observations were conducted at a location approximately 1 mm from the center of the disk. Additionally, cross-sectional observations and surface observations

after laser treatment were carried out using a scanning electron microscope (SEM) Hitachi Su-8000 operating under an accelerating voltage of 10 kV. The images were taken in secondary electron (SE) and backscatter electron (BSE) modes. The hardness distribution of the HPT-processed samples was measured with a microhardness tester (FM300, Future-tech Corp.) under a load of 200 gf and a dwell time of 15 seconds. Tensile tests were conducted on a Zwick universal testing machine with an initial strain rate of 1.0×10^{-3} s^{-1}. Two tensile specimens were cut from each disk sample with a gauge length of 2.0 mm, width of 1.0 mm and thickness of 0.65 mm. The stress-strain curves were plotted for each specimen and the ultimate tensile strengths were derived directly from the curves. The phase structures were examined using an X-ray Diffractometer (D8, Bruker, USA) with Cu-Kα radiation ($\lambda = 0.154$ nm).

In preparing samples for laser surface modification, the N0, N1, N5 and N20 samples were ground with sandpaper to remove burrs and they were then polished to a final surface roughness of about 60 ± 6 nm before laser treatments. The surfaces of the initial solution-treated samples (N0) and HPT-processed samples (N1, N5 and N20) were then modified by laser surface texturing with various laser powers (1~5 W), scan rates (25~150 mm/s) and holding times (0~14 days). The modification process was carried out using a fiber laser system (SPI G3, UK) with a wavelength of 1064 nm, a frequency of 50 kHz, a laser spot diameter of 40 μm and a pulse duration of more than 10 ns. To investigate the effects of the laser processing parameters on the hydrophilic/hydrophobic properties of the TNTZ samples, the contact angles of the laser-modified surfaces were measured using deionized water droplets with a volume of 0.5 μl. To ensure the reliability of the measurements, the contact angle was measured three times for each sample with the three measurements averaged to obtain a representative result. In addition, the surface roughness of all laser-modified samples was measured with an Alpha step profiler (D-300, KLA) with a scanning speed of 0.4 mm/s, a scan line length of 5 mm and a load of 10 mg.

The laser-modified N0 and N20 samples were held for more than 14 days and then subjected to corrosion testing. To evaluate the effect of the hydrophobic surface induced by laser modification on

the corrosion performance, N0, N1, N5 and N20 samples (all with a hydrophilic surface) were also subjected to corrosion testing. The corrosion resistance was measured on an electrochemical work-station (CHI 614E) using 0.9% NaCl at a temperature of 37 °C. The Tafel potential was measured over the range of -0.8 V to 2V at a scanning rate of 0.001 V/s. The wear resistance properties of samples were evaluated using an abrasion testing machine (POD FM800 10NT) fitted with a stainless-steel wear wheel with a diameter of 1 mm. The rotational speed of the wheel was set as 1146 rpm, the normal contact load was set as 1000 g and the total number of wear cycles was set as 100. The wear tests were performed using water as the wet abrasion medium for each sample.

3. Experimental results

3.1. Microstructure development in initial solution-treated and HPT-processed TNTZ samples

Figure 1 presents OM images showing the microstructures of the solution-treated (N0) and HPT-processed N1, N5 and N20 samples at the central areas of the disks. The N0 sample shows a coarse-grained microstructure with an average grain size of ~370 μm. After 1 turn of HPT processing the microstructure remained as coarse grains but after 5 and 20 turns significant grain refinement was observed. For these samples, the individual grains were not found under the low magnification of OM but the flow tendency was apparent due to the shear stress associated with the torsional straining. Compared to the solution-treated sample (N0), the HPT samples showed the emergence of ultra-fine grains as the number of revolutions increased to 5 and 20 turns. Figure 2 shows a high-resolution TEM image of the ultra-fine grain structure in the N20 sample. The SAED pattern indicates numerous high-angle grain boundaries of ultrafine grains and the grain size was measured as less than 100 nm.

Figure 3 shows cross-sectional observations of N20 samples with subsequent laser treatment (5 W, 50 mm/s). In Fig. 3(a), the top surface of the sample is the laser-treated surface and it is possible to see the microstructure change from the top to the bottom area of the image. In the top area of Fig. 3(a), a coarse microstructure with a grain size of around 1 μm is observed due to the thermal effects from the laser power, but nevertheless this reasonably coarse grain size is significantly smaller than

the grain size of ~370 μm in the N0 sample. The bottom area of Fig. 3(a) shows that the microstructure retains the fine grain structures developed from HPT. The phenomenon of a microstructural gradient introduced by laser power is similar to an earlier report [24]. The white protrusions on the surface of the laser-treated N20 sample are present in the TEM image of Fig. 3(a) and they were analyzed by SEM and EDS. Fig 3(b) displays multiple spectrum analyses of the laser-treated N20 sample surface, and the result of spectrum 3 in Fig. 3(c) shows that the white protrusions exhibits a denser oxygen signal and trace amounts of the Ti, Nb and Ta elements. Therefore, it is evident that there is oxide formation on the laser-treated surface.

3.2. Mechanical properties of initial solution-treated and HPT-processed TNTZ samples

Figure 4 shows the Vickers microhardness profiles of the HPT-processed TNTZ alloy samples after 1, 5 and 20 turns. The dashed line represents the microhardness value ~233 Hv for the initial solution-treated sample N0. All of the HPT-processed samples exhibit a higher hardness than the solution-treated sample. For samples with the fewer turns (N1 and N5), the hardness values show lower values in the central region and higher values in the edge region. However, for samples with a high number of turns (N20), the hardness distribution is more uniform and shows no obvious hardness reduction in the center of the disk. The average microhardness values of the N1, N5 and N20 samples were 280, 320 and 340 Hv corresponding to a hardness increase of 20%, 37% and 45%, respectively, with respect to the solution-treated sample.

Figure 5 shows the stress-strain curves of the N0, N1, N5 and N20 samples. The solution-treated sample had a maximum tensile strength of about 590 MPa but by contrast the HPT-processed N1, N5 and N20 samples had far higher maximum tensile strengths of 1280, 1370 and 1410 MPa respectively. Thus, the HPT processing not only refined the grain size but also improved the mechanical properties of hardness and tensile strength of the TNTZ alloy.

3.3. XRD results for initial solution-treated and HPT-processed TNTZ samples

Figure 6 shows the XRD patterns of the N0, N1, N5 and N20 samples. The initial solution-treated TNTZ sample (N0) had a β-phase structure with no detectable presence of the α phase. The HPT samples retained a similar β-phase structure but, as the number of turns increased, the intensity of the main β-phase peak increased while the peak width also increased due to the grain refinement.

3.4. Surface roughness of laser-modified TNTZ samples processed using different laser powers and scan rates

Figure 7 shows the surface roughness values of the solution-treated and HPT-processed TNTZ samples after laser surface modification using laser powers of 1, 2 and 5 W and scan rates of 25, 50, 100 and 150 mm/s, respectively. All samples had a similar low roughness for a laser power of less than 2 W. However, as the laser power increased to 5 W, the surface roughness increased by several hundred times for all four samples, particularly at lower scan rates. For the HPT-processed 20 turns sample, the surface roughness following laser treatment with a power of 5 W and a scan rate of 150 mm/s was around 5-6 times higher than for the N0 sample with the same laser treatment conditions, as shown in Fig.7 (a) and (d).

Figure 8 compares the SEM surface morphologies of the two samples modified using a scan speed of 50 mm/s. The N0 sample contained a small number of ordered orientation cracks originating from the horizontal scan tracks. For the N20 sample, the number of staggered cracks was greatly increased which produced the higher surface roughness observed in Fig. 7(d) compared to Fig. 7(a). The N20 sample had a much finer grain size of less than 100 nm than the N0 sample with ~370 μm due to the grain refinement from HPT processing and the N20 sample also displayed more randomly-oriented solidification cracks after the laser treatment.

3.5. Variation of contact angle with holding time for laser-modified TNTZ samples processed using different laser powers

The contact angles of the laser-modified samples were measured daily over a 14-day holding

period in air. As shown in Fig. 9, all the laser-treated samples experienced a transition from an initial hydrophilic surface to a steady-state hydrophobic surface with an increased holding time. For lower laser powers of 1 and 2 W, a transition to the hydrophobic surface with a contact angle around 90-100° occurred in all samples within 2 days. For the highest power of 5 W, the surface characteristics of the N1 and N20 samples transformed from hydrophilic to hydrophobic surfaces within 2~3 days. However, compared to samples processed at the lower laser powers of 1 W and 2 W, the degree of hydrophobicity was greatly increased in samples processed at the higher laser power of 5 W with a maximum contact angle of around 140°.

Fig. 10 shows a tendency for the carbon content to increase whereas the oxygen content was reduced with the holding time in the laser-treated TNTZ samples. All four samples were processed using a laser power of 5 W and scan speed of 25 mm/s. These surface compositional changes during the 14-day holding period are similar to observations reported on laser-treated CP-Ti and the Ti64 alloy [25] and they confirm the surface oxide formation leading to surface hydrophobicity. Noting the difference between the four samples in Fig. 10, it is apparent that the laser-treated N5 and N20 samples have a higher C content of around 13 at% and a lower O content of approximately 32.5 at% after 14 days of holding time. Thus, the laser-treated HPT samples have surface features with higher C content and lower O content besides higher surface roughness and these characteristics can bring beneficial effects in enhancing the hydrophobicity of the TNTZ samples.

3.6. Effect of different laser and HPT treatments on corrosion properties

Figure 11 shows the Tafel curves for the N0, N1, N5 and N20 samples under the conditions without laser treatment and with laser treatment with a laser power of 5 W and a scan rate of 25 mm/s. Figure 11(a) presents the results for the solution-treated (N0) and HPT samples N1, N5 and N20 with no laser treatment whereas Figs. 11(b) and (c) show the results for the laser-treated N0, N1, N5 and N20 samples after holding for 0 day and 14 days, respectively. The corrosion potential and current data in Fig. 11 were plotted in Fig. 12. Thus, for samples without laser treatment, Fig. 11(a) and Fig.

12(a) demonstrate that the N0 sample has a lower corrosion potential (-0.422 V) than the N20 sample (-0.349 V). Furthermore, the N0 sample has a higher corrosion current than the N20 sample. Obviously, without laser surface treatment the HTP-processed N20 sample has a better corrosion resistance than the solution-treated N0 sample. Following laser treatment, Fig. 12(c) shows that the corrosion potential of the laser-treated N0 sample is -0.191 V after 14 days of holding, and this is smaller than for the N0 sample without laser treatment which was -0.422 V, as shown in Fig. 12(a).

The corrosion resistance of the N20 HPT-proceed sample also improved after laser surface treatment. Fig. 12(a) and (c) show that the corrosion potential of the N20 sample increases from -0.349 V without laser treatment to -0.158 V after laser treatment and 14 days holding, whereas the corrosion current decreases from 1×10^{-8} A without laser treatment to 3.2×10^{-9} A after laser treatment and 0 day holding and 1.2×10^{-9} A after laser treatment and 14 days holding. These results demonstrate that the hydrophobic surface of the laser-treated HPT samples with 0 day and 14 days holding contribute to a corrosion resistance improvement.

3.7. Effect of different laser and HPT treatments on abrasion properties

Figure 13 shows the variation of the coefficient of friction with the number of sliding cycles for the N0, N1, N5 and N20 samples with and without laser modification, respectively. In the absence of laser modification, the friction coefficient of the initial solution-treated sample N0 is similar to that of all HPT-processed samples N1, N5 and N20. All samples show a lower friction coefficient following laser surface treatment than those without laser treatment. For example, the friction coefficient of the N0 sample is reduced from 0.122 without laser treatment to 0.04 after laser treatment and 14 days holding, as shown in Fig. 13(a). Fig. 13(b-d) shows that the wear resistance of all HPT-processed samples improved immediately after laser treatment with 0 day holding and there was further improvement after 14-day holding. For example, the friction coefficient of the N20 sample was reduced from 0.134 without laser treatment to 0.093 after laser treatment and 0 day holding and 0.082 after laser treatment and 14 days holding. The smaller friction coefficient in the samples after

laser treatment and 14 days of holding appears to be related to the emergence of the hydrophobic surface property.

4. Discussion

The results presented in Figs 1 to 4 show that HPT processing leads to a significant grain refinement which in turn produces a higher microhardness value. The grain size in the TNTZ alloy was reduced from ~370 μm in the initial solution-treated alloy to less than 100 nm after 20 turns of HPT processing. Both the degree of grain refinement and the extent of the microhardness enhancement increase with increasing numbers of HPT turns due to the corresponding increase in the shear strain applied to the samples. The microhardness value of the initial solution-treated sample was 233 Hv and the average microhardness value for the 20 turns sample was 340 Hv. The tensile results in Fig. 5 show that the HPT-processed TNTZ N20 sample not only has higher strength (~1410 MPa) but also reasonable ductility (30%). The X-ray results in Fig. 6 demonstrate that the TNTZ alloy has a β-phase structure with no detectable presence of an α phase before and after HPT processing. Since the β phase is beneficial in improving the biocompatibility of Ti-based alloys with human bone [11], the HPT-processed TNTZ N20 sample with its high hardness, high tensile strength and β-phase structure appears to be an exceptionally promising candidate for biomedical applications.

Applying a laser surface treatment to the HPT-processed TNTZ alloy is expected to generate a surface texture to modify the surface characteristics and improve the corrosion performance and wear resistance, where these are all important factors for high performance bioimplant applications. In Fig. 8, the N20 sample displayed more randomly-oriented solidification cracks after the laser treatment. It is noted that the present results of the solidification behavior for the nano-structured TNTZ sample are consistent with results reported for laser-irradiated nano-sized cerium dioxide [26].

The degree of hydrophobicity was greatly increased in samples processed at a higher laser power (5 W) with a maximum contact angle of around 140°, as shown in Fig. 9(c). As described in an earlier report [27], this greater hydrophobicity can be attributed to the higher surface roughness of the

samples processed at a higher laser power. There are reports of a 316L stainless steel surface transitioning progressively from superhydrophilic after the laser texturing process to hydrophobic after aging in air for 7-14 days [28]. It was also suggested that the melted and resolidified metal oxide can absorb organic compounds in ambient air leading to surface superhydrophobicity [29-31]. To confirm a similar mechanism for the transition from a hydrophilic to hydrophobic surface in laser-treated TNTZ samples, the variation of the carbon and oxygen contents in the laser-treated N0, N1, N5 and N20 samples were measured over a 14 days holding period when exposed to the ambient environment. The results in Fig. 10 demonstrate that the carbon content was increased whereas the oxygen content was reduced with the holding time in all four samples, thereby confirming that the surface oxide formation leads to a surface characteristic transition from hydrophilicity to hydrophobicity.

From the Tafel curves in Fig. 11 and the corresponding current potential and corrosion current in Fig. 12, it is concluded that the corrosion resistance of the N0 sample was improved markedly following the initial laser treatment process and was continually improved with the holding time. The N20 HPT samples demonstrated a similar corrosion resistance improvement tendency after the laser surface treatment with holdings of 0 days and 14 days. The improved corrosion resistance with holding time is attributed to the emergence of the hydrophobic surface which suppresses pitting corrosion [32].

It was noticed that the laser-treated N20 sample always has a larger corrosion potential and smaller corrosion current than the laser-treated N0 sample. The N20 HPT sample has a grain size of less than 100 nm (Fig. 2) and the surface area of the laser-treated N20 sample has a very fine grain size of ~1 μm (Fig. 3) with the exposure to laser power. Whereas the N0 sample has a very coarse grain structure with an average grain size of ~370 μm (Fig. 1), the laser-treated surface area of the N0 sample should have an even coarser grain size due to inherent heating from the laser power. From a comparison between the laser-treated N0 and N20 samples, it is concluded that there is a grain size effect on the laser treatment and corrosion behavior, such that the laser-treated N20 sample with a

fine grain structure shows an improved corrosion resistance compared with the laser-treated N0 sample with a coarse grain structure. There are several reports documenting the effect of grain refinement on the material corrosion behavior in an Al alloy [33], a CuNi alloy [34],and in a Ni-based alloy [35]. It was generally agreed that refined grains improve the corrosion resistance of deformed alloys [33]. Fig. 12 shows that both the laser-treated N0 and N20 samples have improved corrosion resistance during 0-14 days holding due to the emergence of the hydrophobic surface. In addition, Fig. 9(c) demonstrates that the laser-treated samples N1 and N20 reach the hydrophobic steady state more rapidly than the laser-treated N0 sample, which suggest that the laser-treated HPT samples should reach good corrosion resistance more quickly than the laser-treated N0 sample. Hence, it is concluded that a combination of HPT processing with subsequent laser treatment not only improves the corrosion resistance of the TNTZ alloy but also reduces the time required to achieve the superior corrosion resistance.

The wear resistance was evaluated in samples that experienced HPT processing and laser treatment with 0 and 14 days holding. The results in Fig. 13 show the friction coefficient in the N20 sample was reduced from 0.134 without laser treatment to 0.093 after laser treatment and 0 day holding and to 0.082 after laser treatment and 14 days holding. The smaller friction coefficient in samples after laser treatment and 14 days holding appears to be related to the emergence of the hydrophobic surface property. The oxide formation occurs on the laser-treated surface and it also contributes to improving the corrosion and wear resistance. According to published results, the enhanced corrosion and wear properties may be obtained due to the oxide layers compared with the original material. For example, TiO_2 [36] resulted in a 95% decrease in corrosion current from 254 to 12 nA/cm^2 and a 75% reduction in friction coefficient from 0.64 to 0.16. For TaO_2 [37] there was a 71% reduction in corrosion current from 1.664×10^{-8} to 4.739×10^{-9} A/cm^2 and a 16.9% decrease in friction coefficient from 0.183 to 0.152. Similar trends were also observed for Nb_2O_5 [38, 39] and ZrO_2 [40].

5. Summary and conclusions

This study evaluated the mechanical, corrosion and wear properties of Ti–29Nb–13Ta–4.6Zr (TNTZ) alloy samples processed by a combination of HPT and laser surface modification. The experimental results support the following conclusions:

(1) HPT processing produced a grain refinement in the microstructure which enhanced the mechanical properties of the TNTZ alloy. The extent of the grain refinement increased with increasing numbers of torsional revolutions. The hardness of the N20 HPT sample was about 45% higher than for the solution-treated sample N0.

(2) Laser treatment with a higher laser power (5 W) and lower scan rate (25 mm/s) led to an increased surface roughness. Following the laser treatment process, all samples experienced a transition from a hydrophilic surface to a hydrophobic surface as the holding time increased, and this was accompanied by a gradual increase in the carbon content and a reduction in the oxygen content.

(3) The laser treatment gave a significant improvement in the corrosion resistance of the fine-grained TNTZ alloy. In the steady-state hydrophobic condition, the corrosion potential of the N20 sample increased from -0.349 V to -0.158 V whereas the corrosion current decreased from 1×10^{-8} A to 1.2×10^{-9} A.

(4) The hydrophobic surface induced by the laser treatment and subsequent holding improved the wear resistance of the TNTZ alloy.

Funding The authors received financial support provided by the National Science and Technology Council, ROC, under Project No. NSTC 111-2927-I-020-501 and by the Royal Society in the UK under Grant No. IEC\R3\193025.

Data availability All data generated or analyzed during this study are included in the present article

Declarations

Ethics approval Not applicable.

Consent to participate Not applicable.

Consent for publication Not applicable.

Competing interests The authors declare no competing interests.

Author contribution H.K. Lin: writing, review, and funding acquisition. Tsai-Hsuan Hsieh: investigation, formal analysis and data collection. Yi-Hong Cheng: data collection and visualization. Piotr Bazamik: formal analysis and data collection. Chuan Ting Wang: resources and data collection. Yi Huang: writing, review, and funding acquisition. Jing Ye: data collection and visualization. Amor Abdelkader: resources and review. T.G. Langdon: writing and review.

Reference

[1] A. Cremasco, A.D. Messias, A.R. Esposito, E.A.d.R. Duek, R. Caram, Effects of alloying elements on the cytotoxic response of titanium alloys, Materials Science and Engineering: C 31(5) (2011) 833-839.

[2] M. Jasty, Clinical reviews: Particulate debris and failure of total hip replacements, Journal of Applied Biomaterials 4(3) (1993) 273-276.

[3] L.-Y. Chen, Y.-W. Cui, L.C. Zhang, Recent Development in Beta Titanium Alloys for Biomedical Applications, Metals 10(9) (2020) 1139.

[4] M. Karthega, V. Raman, N. Rajendran, Influence of potential on the electrochemical behaviour of β titanium alloys in Hank's solution, Acta Biomaterialia 3(6) (2007) 1019-1023.

[5] M. Niinomi, Fatigue performance and cyto-toxicity of low rigidity titanium alloy, Ti–29Nb–13Ta–4.6Zr, Biomaterials 24(16) (2003) 2673-2683.

[6] A.H. Hussein, M.A.H. Gepreel, M.K. Gouda, A.M. Hefnawy, S.H. Kandil, Biocompatibility of new Ti–Nb–Ta base alloys, Materials Science and Engineering: C 61 (2016) 574-578.

[7] M. Niinomi, Mechanical properties of biomedical titanium alloys, Materials Science and Engineering: A 243(1) (1998) 231-236.

[8] A.E. Medvedev, A. Molotnikov, R. Lapovok, R. Zeller, S. Berner, P. Habersetzer, F. Dalla Torre, Microstructure and mechanical properties of Ti–15Zr alloy used as dental implant material, Journal of the Mechanical Behavior of Biomedical Materials 62 (2016) 384-398.

[9] M. Geetha, A.K. Singh, R. Asokamani, A.K. Gogia, Ti based biomaterials, the ultimate choice for orthopaedic implants – A review, Progress in Materials Science 54(3) (2009) 397-425.

[10] J.P. Luo, Y.J. Huang, J.Y. Xu, J.F. Sun, M.S. Dargusch, C.H. Hou, L. Ren, R.Z. Wang, T. Ebel, M. Yan, Additively manufactured biomedical Ti-Nb-Ta-Zr lattices with tunable Young's modulus: Mechanical property, biocompatibility, and proteomics analysis, Materials Science & Engineering C, Materials for biological applications 114 (2020) 110903.

[11] Y. Huang, S. Mortier, P.H.R. Pereira, P. Bazarnik, M. Lewandowska, T.G. Langdon, Thermal stability and mechanical properties of HPT-processed CP-Ti, IOP Conference Series: Materials Science and Engineering, IOP Publishing, 2017, p. 012012.

[12] H. Shahmir, J. He, Z. Lu, M. Kawasaki, T.G. Langdon, Effect of annealing on mechanical properties of a nanocrystalline CoCrFeNiMn high-entropy alloy processed by high-pressure torsion, Materials Science and Engineering: A 676 (2016) 294-303.

[13] D. Gunderov, S. Prokoshkin, A. Churakova, V. Sheremetyev, I. Ramazanov, Effect of HPT and accumulative HPT on structure formation and microhardness of the novel Ti18Zr15Nb alloy, Materials Letters 283 (2021) 128819.
[14] R. Mishra, R. Balasubramaniam, Effect of nanocrystalline grain size on the electrochemical and corrosion behavior of nickel, Corrosion Science 46(12) (2004) 3019-3029.
[15] B.H. Luo, P.W. Shum, Z.F. Zhou, K.Y. Li, Preparation of hydrophobic surface on steel by patterning using laser ablation process, Surface and Coatings Technology 204(8) (2010) 1180-1185.
[16] M.H. Kwon, H.S. Shin, C.N. Chu, Fabrication of a super-hydrophobic surface on metal using laser ablation and electrodeposition, Applied Surface Science 288 (2014) 222-228.
[17] O. Raimbault, S. Benayoun, K. Anselme, C. Mauclair, T. Bourgade, A.M. Kietzig, P.L. Girard-Lauriault, S. Valette, C. Donnet, The effects of femtosecond laser-textured Ti-6Al-4V on wettability and cell response, Materials Science and Engineering: C 69 (2016) 311-320.
[18] W.A. Loesberg, J. te Riet, F.C.M.J.M. van Delft, P. Schön, C.G. Figdor, S. Speller, J.J.W.A. van Loon, X.F. Walboomers, J.A. Jansen, The threshold at which substrate nanogroove dimensions may influence fibroblast alignment and adhesion, Biomaterials 28(27) (2007) 3944-3951.
[19] Y.H. Chen, W.S. Chuang, J.C. Huang, X. Wang, H.S. Chou, Y.J. Lai, P.H. Lin, On the bio-corrosion and biocompatibility of TiTaNb medium entropy alloy films, Applied Surface Science 508 (2020) 145307.
[20] S.K. Kolawole, W. Hai, S. Zhang, Z. Sun, M.A. Siddiqui, I. Ullah, W. Song, F. Witte, K.Yang, Preliminary study of microstructure, mechanical properties and corrosion resistance of antibacterial Ti-15Zr-xCu alloy for dental application, Journal of Materials Science & Technology 50 (2020) 31-43.
[21] Y.L. Zhou, M. Niinomi, T. Akahori, H. Fukui, H. Toda, Corrosion resistance and biocompatibility of Ti–Ta alloys for biomedical applications, Materials Science and Engineering: A 398(1-2) (2005) 28-36.
[22] S. Li, R. Yang, S. Li, Y. Hao, Y. Cui, M. Niinomi, Z.X. Guo, Wear characteristics of Ti–Nb–Ta–Zr and Ti–6Al–4V alloys for biomedical applications, Wear 257(9-10) (2004) 869-876.
[23] R.B. Figueiredo, P.R. Cetlin, T.G. Langdon, Using finite element modeling to examine the flow processes in quasi-constrained high-pressure torsion, Materials Science and Engineering: A 528(28) (2011) 8198-8204.
[24] A. Baumard, D. Ayrault, O. Fandeur, C. Bordreuil, F. Deschaux-Beaume, Design, Numerical prediction of grain structure formation during laser powder bed fusion of 316 L stainless steel, Materials & Design 199 (2021) 109434.
[25] H.K. Lin, Y.H. Cheng, G.Y. Li, Y.C. Chen, P. Bazarnik, J. Muzy, Y. Huang, T.G. Langdon, Study on the Surface Modification of Nanostructured Ti Alloys and Coarse-Grained Ti Alloys, Metals 12(6) (2022) 948.
[26] D. Manara, K. Popa, D. Robba, L. Fongaro, J.-Y. Colle, A. Bulgheroni, Infrared laser absorption and melting behaviour of nano-sized cerium dioxide: A laser heating study, Journal of the European Ceramic Society 41(2) (2021) 1384-1390.
[27] H.K. Lin, G.Y. Li, S. Mortier, P. Bazarnik, Y. Huang, M. Lewandowska, T.G. Langdon, Processing of CP-Ti by high-pressure torsion and the effect of surface modification using a post-HPT laser treatment, Journal of Alloys and Compounds 784 (2019) 653-659.
[28] C.-L. Chang, M.T. Hsu, H.K. Lin, K. Chuang, J. Huang, Effects of metal film coatings on surface properties of laser-textured stainless steel, Surface and Coatings Technology 461 (2023) 129446.
[29] S. Takeda, M. Fukawa, Y. Hayashi, K. Matsumoto, Surface OH group governing adsorption properties of metal oxide films, Thin Solid Films 339(1) (1999) 220-224.
[30] M. Ortiz-Morales, C. Frausto-Reyes, J.J. Soto-Bernal, S.E. Acosta-Ortiz, R. Gonzalez-Mota, I. Rosales-Candelas, Infrared nanosecond pulsed laser irradiation of stainless steel: Micro iron-oxide zones generation, Spectrochimica Acta Part A: Molecular and Biomolecular Spectroscopy 128 (2014) 681-685.

[31] L. Zhuang, W. Zhang, Y. Zhao, H. Shen, H. Lin, J. Liang, Preparation and characterization of Fe3O4 particles with novel nanosheets morphology and magnetochromatic property by a modified solvothermal method, Scientific Reports 5 (2015) 9320.
[32] W.T. Choi, K. Oh, P.M. Singh, V. Breedveld, D.W. Hess, Hydrophobicity and improved localized corrosion resistance of grain boundary etched stainless steel in chloride-containing environment, Journal of The Electrochemical Society 164(2) (2017) C61.
[33] G. Li, X. Pan, J. Jiang, J. Li, L. Xie, H. Liu, M. Zhang, Achieving ultra-fine grains and high corrosion resistance of Al–Zn–Mg–Cu alloy by ECAP and post cold rolling, Journal of Materials Research and Technology 26 (2023) 7354-7368.
[34] Y. Zhao, L. Peng, H. Xie, W. Zhang, S. Huang, Z. Yang, Z. Li, X. Mi, Enhancing the erosion–corrosion resistance of cupronickel alloy through grain boundary engineering, Corrosion Science 219 (2023) 111228.
[35] J. Lv, Effect of grain size on mechanical property and corrosion resistance of the Ni-based alloy 690, Journal of Materials Science & Technology 34(9) (2018) 1685-1691.
[36] H. Bakhtiari-Zamani, E. Saebnoori, H.R. Bakhsheshi-Rad, F. Berto, Corrosion and Wear Behavior of TiO2/TiN Duplex Coatings on Titanium by Plasma Electrolytic Oxidation and Gas Nitriding, Materials, 15 (2022) 8300.
[37] B. Rahmati, A.A.D. Sarhan, W.J. Basirun, W.A.B.W. Abas, Ceramic tantalum oxide thin film coating to enhance the corrosion and wear characteristics of Ti6Al4V alloy, Journal of Alloys and Compounds 676 (2016) 369-376.
[38] J.A. Moreto, R.V. Gelamo, J.P.L. Nascimento, M. Taryba, J.C.S. Fernandes, Improving the corrosion protection of 2524-T3-Al alloy through reactive sputtering Nb2O5 coatings, Applied Surface Science 556 (2021) 149750.
[39] G. Orozco-Hernández, P.G. Durán, W. Aperador, Tribocorrosion Evaluation of Nb2O5, TiO2, and Nb2O5 + TiO2 Coatings for Medical Applications, Lubricants, 9 (2021) 49.
[40] J. Walkowicz, V. Zavaleyev, E. Dobruchowska, D. Murzynski, N. Donkov, A. Zykova, V. Safonov, S. Yakovin, Corrosion properties of zirconium-based ceramic coatings for micro-bearing and biomedical applications, Journal of Physics: Conference Series, IOP Publishing, 2016, p.012026.

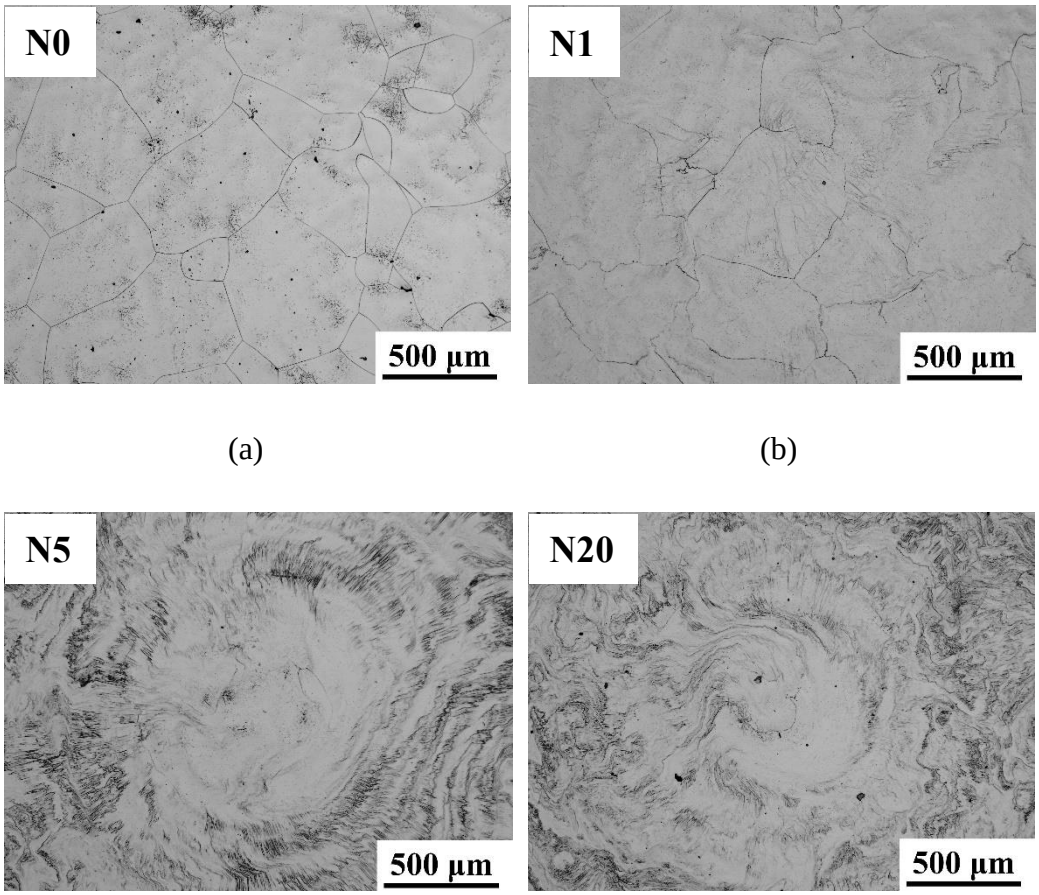

Fig. 1 OM microstructures of: (a) solution-treated N0 sample and (b) N1, (c) N5 and (d) N20 HPT-processed samples.

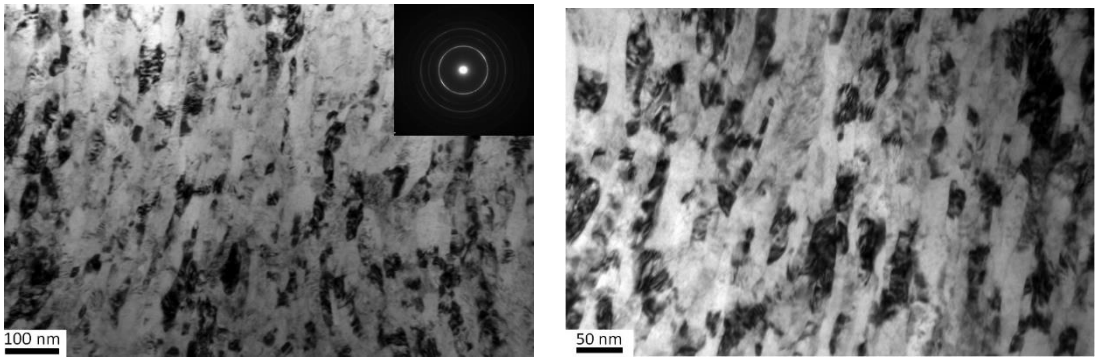

Fig. 2 TEM images of N20 HPT-processed sample (a) lower magnification with SAED pattern inserted and (b) higher magnification.

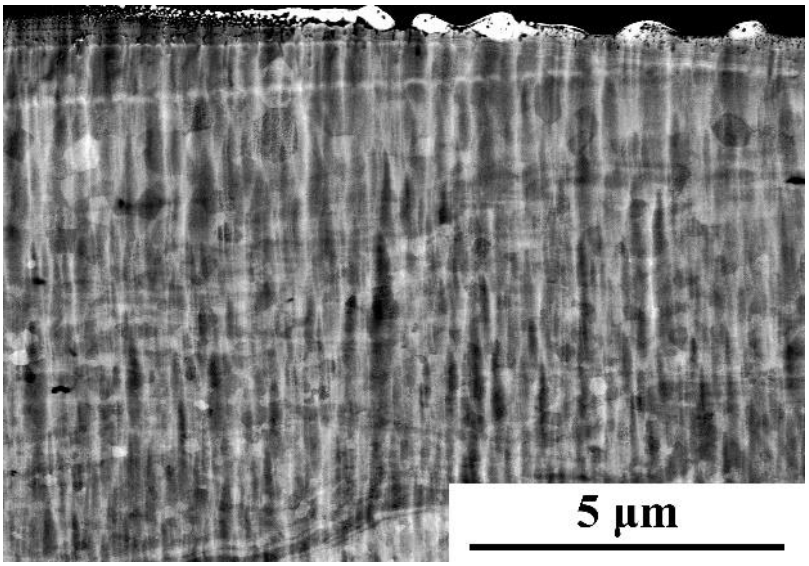

(a)

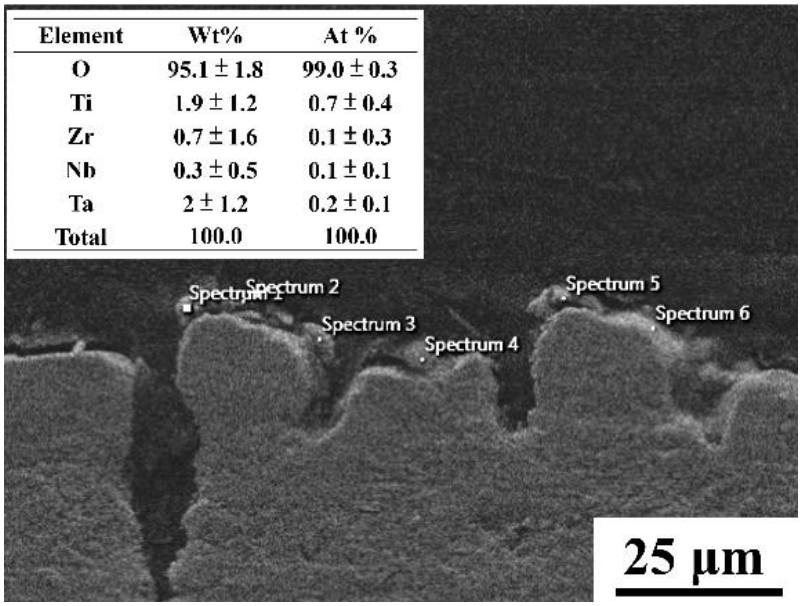

(b)

Fig. 3 N20 HPT-processed sample of (a) SEM cross-section BSE image taken in channeling contrast, (b) SEM image with EDS results.

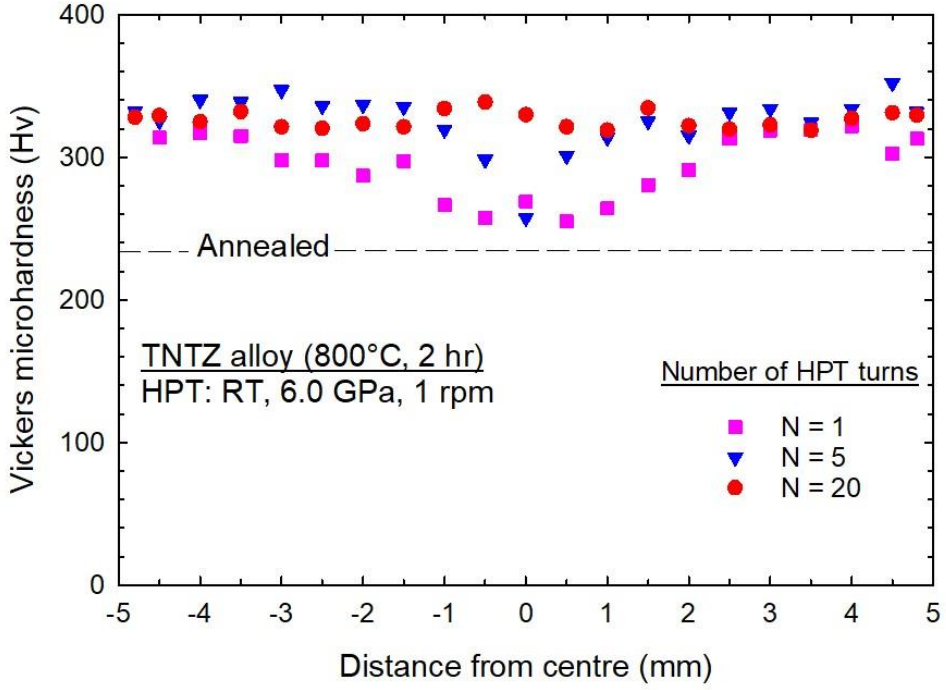

Fig. 4 Microhardness profiles of HPT-processed N1, N5 and N20 samples.

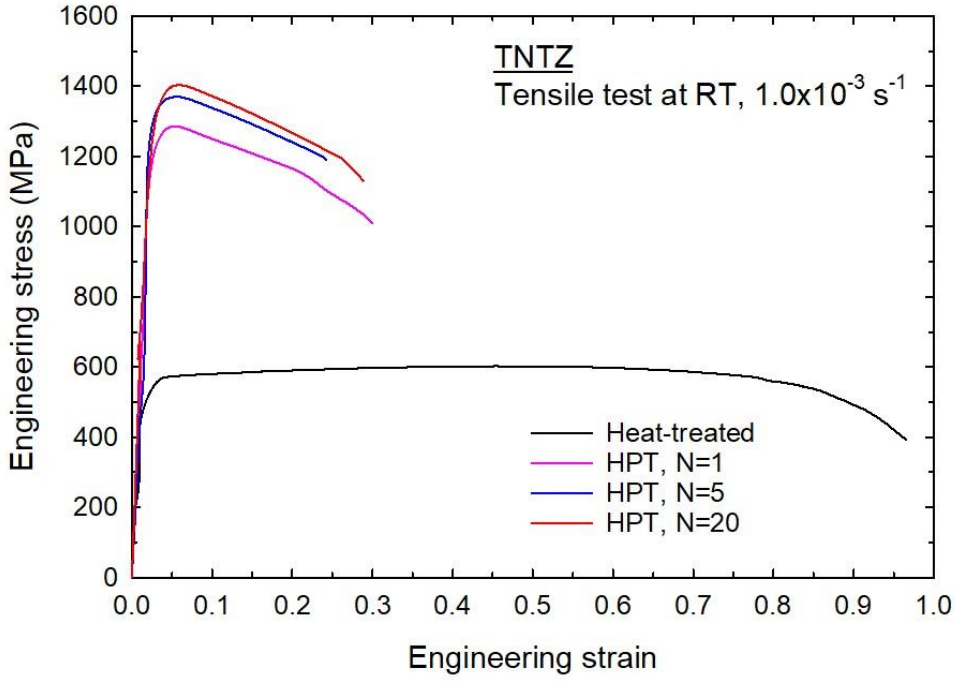

Fig. 5 Tensile properties of solution-treated N0 sample and HPT-processed N1, N5 and N20 samples.

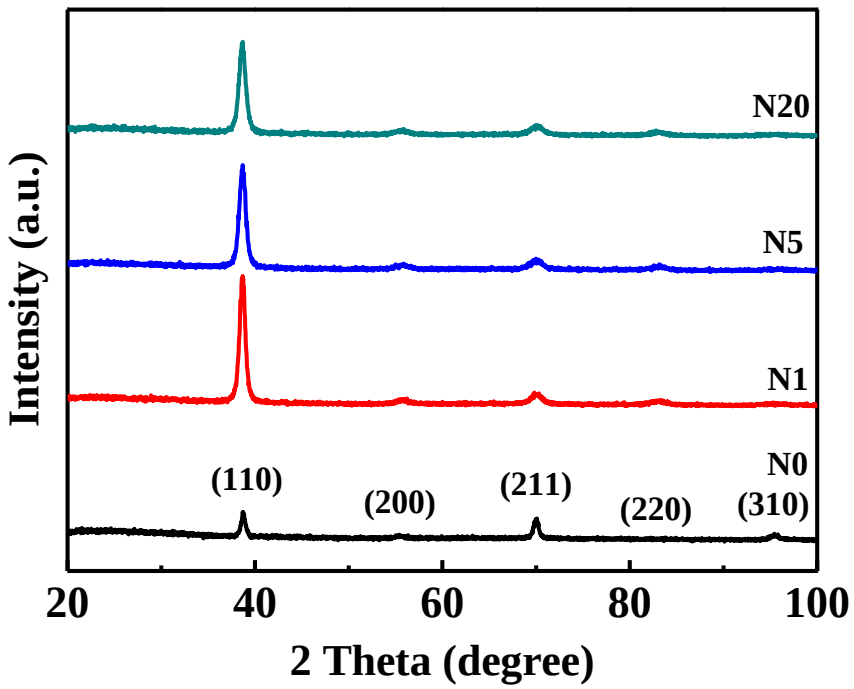

Fig. 6 XRD patterns of solution-treated N0 sample and HPT-processed N1, N5 and N20 samples.

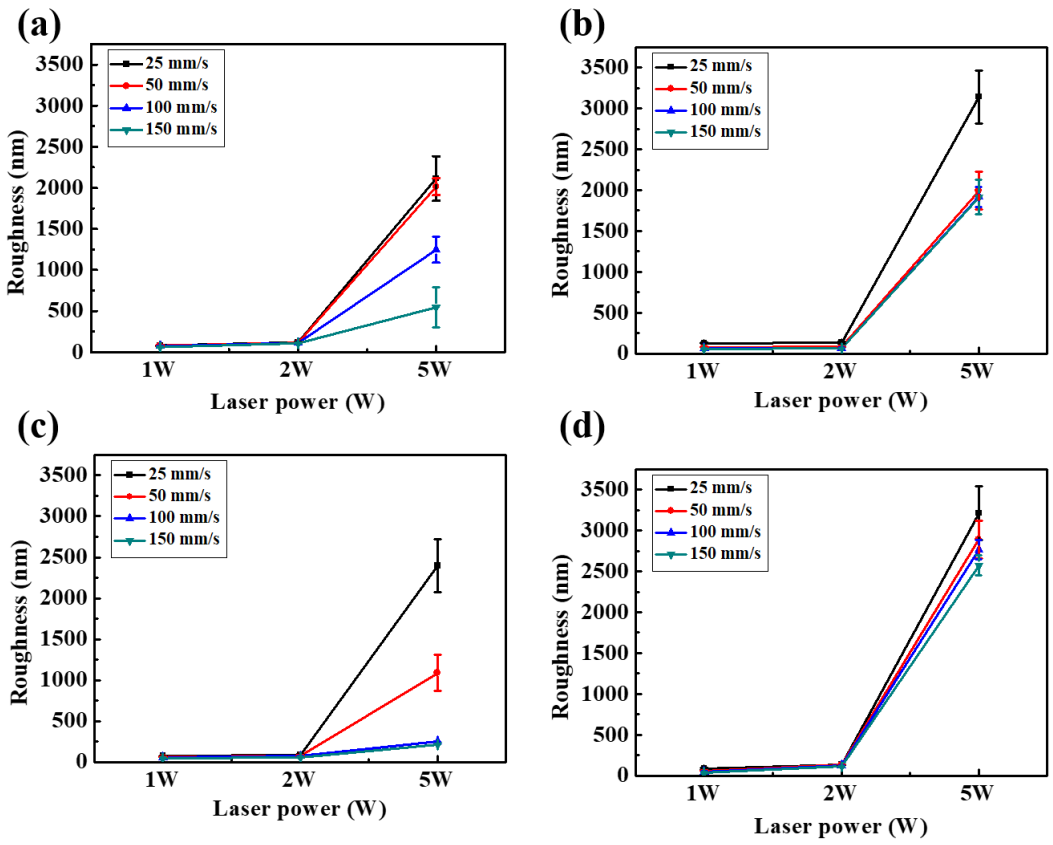

Fig. 7 Surface roughness of different samples following laser surface modification with different powers and scan rates. (a) solution-treated N0 sample and (b) N1, (c) N5 and (d) N20 HPT-processed samples.

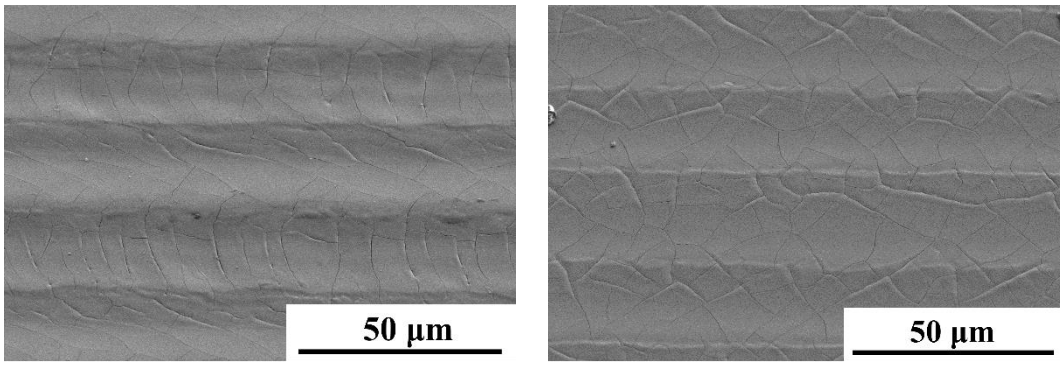

(a) (b)

Fig. 8 SEM surface morphologies of (a) N0 and (b) N20 samples following laser treatment with laser power of 5 W and scanning speed of 50 mm/s.

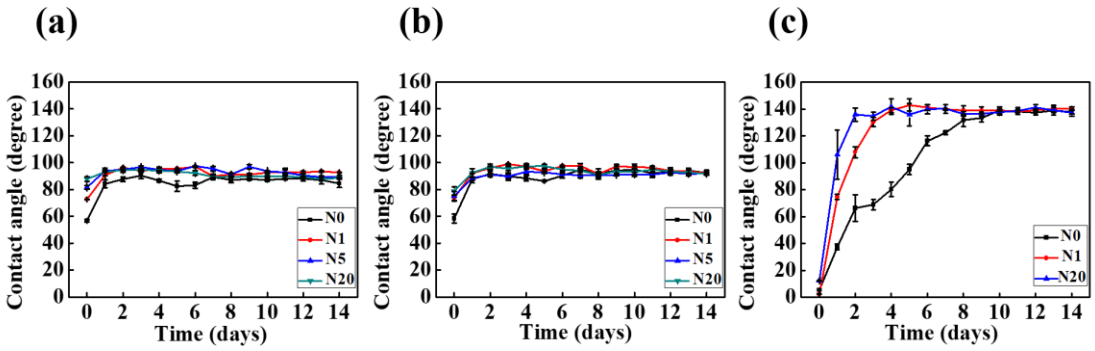

Fig. 9 Variation of contact angle with holding time for solution-treated N0 sample and HPT-processed N1, N5 and N20 samples treated using laser powers of (a) 1 W, (b) 2 W and (c) 5 W with a laser scan rate of 50 mm/s.

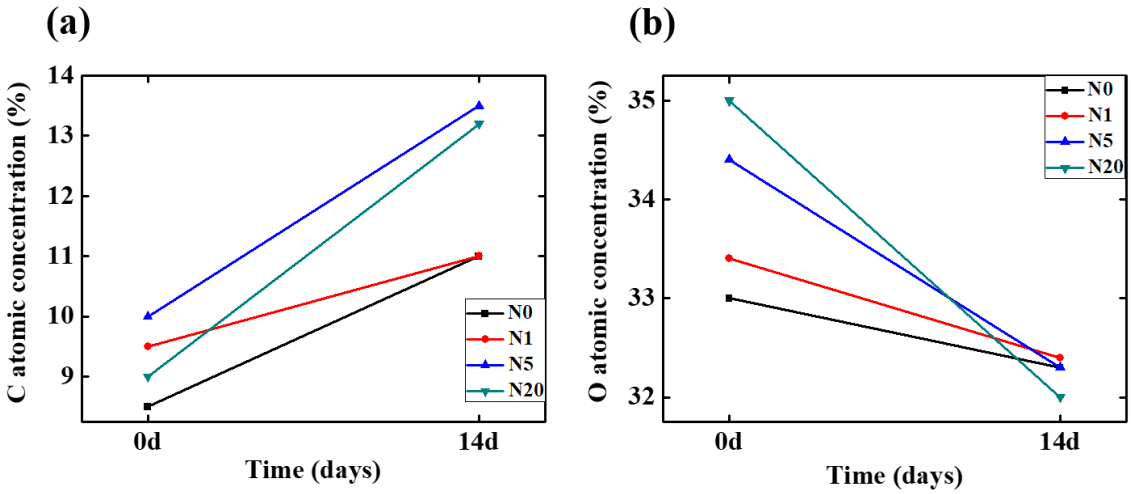

Fig. 10 Change in concentration of chemical elements in laser-modified N0, N1, N5 and N20 samples over holding time: (a) carbon content and (b) oxygen content.

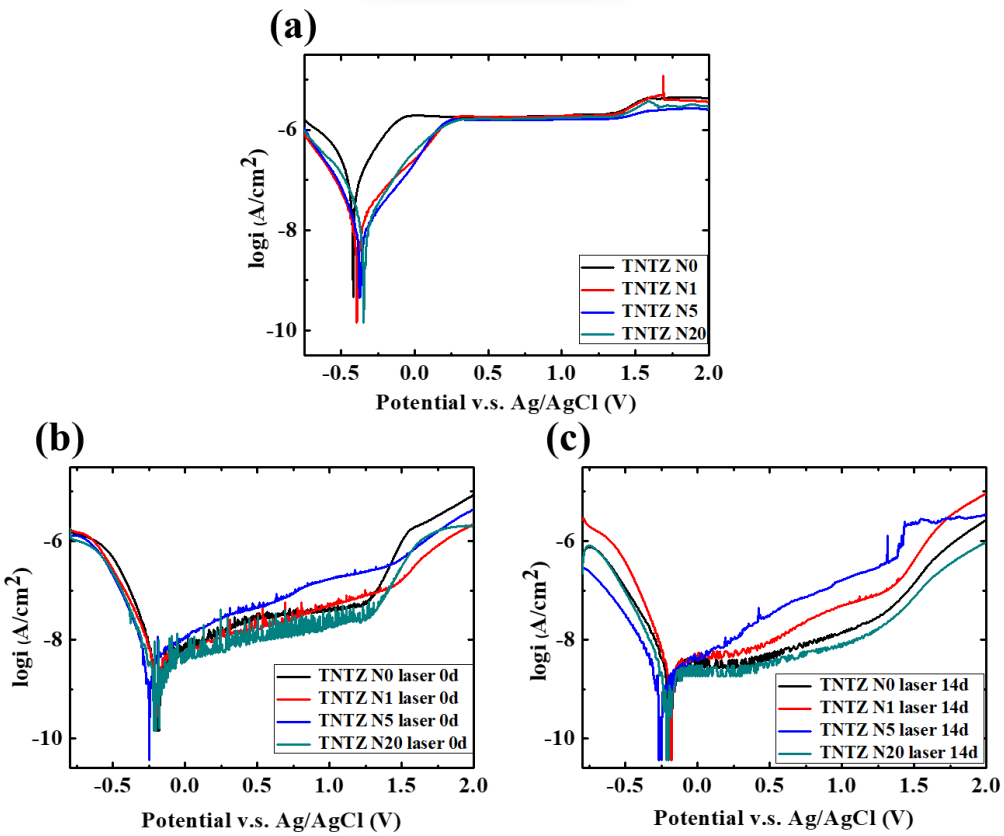

Fig. 11 Tafel curves for N0, N1, N5 and N20 samples after different holding times (a) with no laser treatment and (b) 0 days aging time and (c) 14 days aging time.

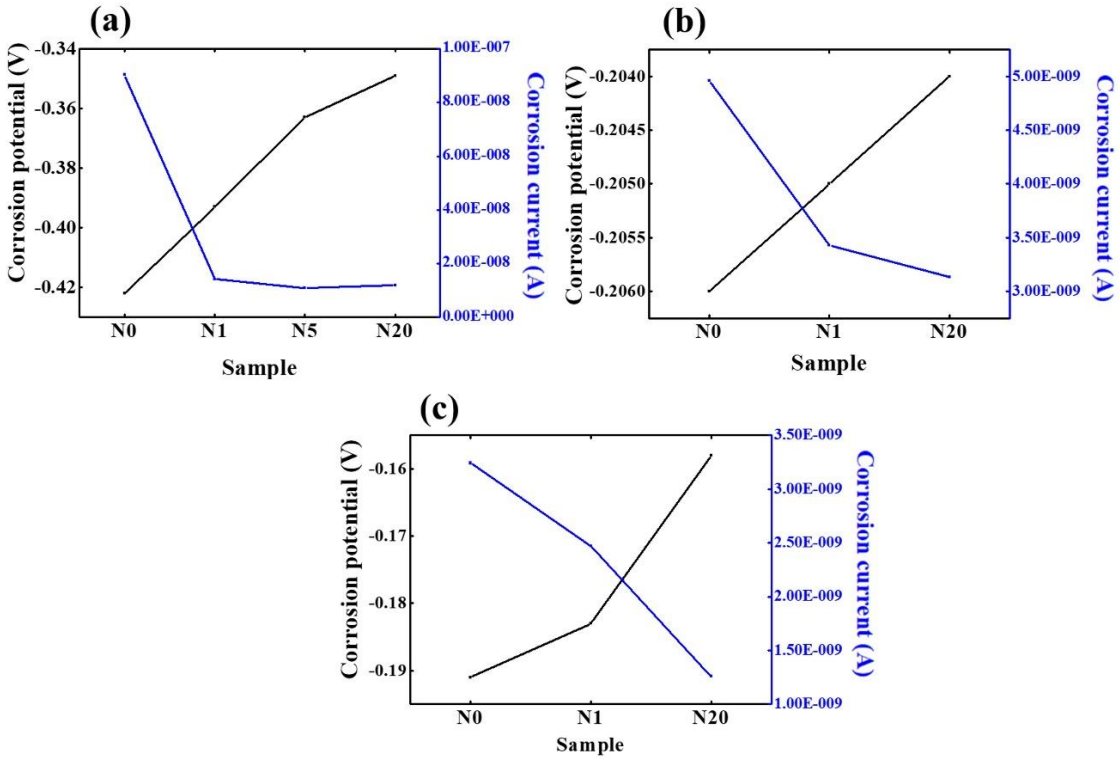

Fig. 12 Variation of corrosion potential and current of the initial solution-treated (N0) and HPT-proceed samples with different holding time for (a) no laser treatment, (b) 0 days and (c) 14 days.

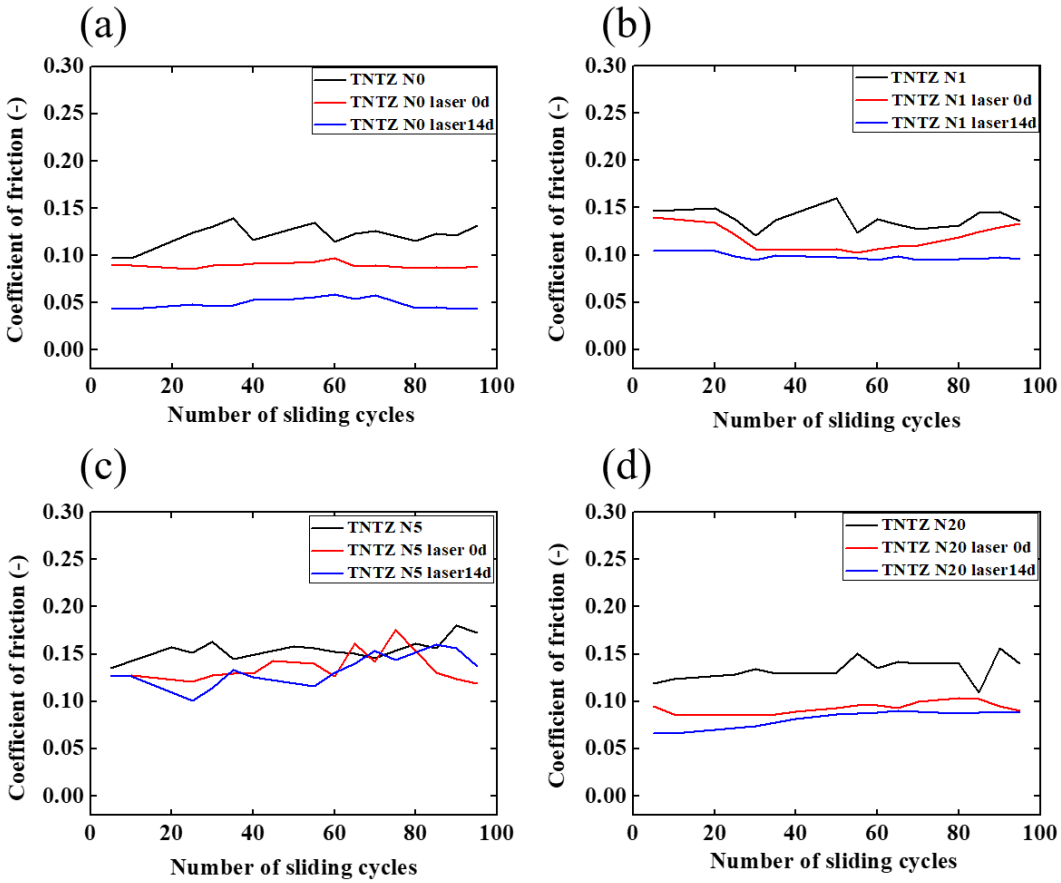

Fig. 13 Variations of the coefficient of friction in the laser modified surface with different holding times for (a) the initial solution-treated (N0), (b) N1, (c) N5 and (d) N20 samples.